A&A 401, 781–796 (2003)
DOI: 10.1051/0004-6361:20030075

Astronomy & Astrophysics

The Asiago Database on Photometric Systems (ADPS)⋆,⋆⋆

II. Band and reddening parameters

M. Fiorucci[1,2] and U. Munari[1,2]

[1] Osservatorio Astronomico di Padova – INAF, Sede di Asiago, 36012 Asiago (VI), Italy
[2] CISAS, Centro Interdipartimentale Studi ed Attività Spaziali "Giuseppe Colombo", Università di Padova, Italy

Received 18 August 2002 / Accepted 14 January 2003

Abstract. The Asiago Database on Photometric Systems (ADPS) is a compilation of basic information and reference data on 201 photometric systems (both ground-based and space-born), available in printed form (Moro & Munari 2000, hereafter Paper I) and electronically (`http://ulisse.pd.astro.it/ADPS`). Seventeen new systems have been added to ADPS since its publication, bringing the total to 218. In this Paper II, band and reddening parameters are homogeneously computed via synthetic photometry for the censed photometric systems with known band transmission profiles (179 systems). Band parameters include various types of wavelengths (mean, peak, Gaussian, and effective according to a series of representative spectral types), widths (width at half maximum, at 80% and 10% of transmission's peak, *FWHM* of the fitting Gaussian, equivalent, and effective for representative spectral types), moment of the 2nd order, skewness and kurtosis indices, and polynomial expressions for the behavior of effective wavelength and effective width as function of black-body temperature. Reddening parameters include $A(\lambda)/A(V)$ for three reddening laws (characterized by $R_V = 5.0$, 3.1 and 2.1) and its range of variability over the HR diagram, the Cardelli et al. (1989) $a(x)$ and $b(x)$ coefficients, second order fits to $A(\lambda)/E_{B-V}$ for three representative spectral types, and polynomial expressions for the behavior of effective wavelength and effective width as function of reddening (for the $R_V = 3.1$ law).

Key words. techniques: photometric – astronomical data bases: miscellaneous – catalogs

1. Introduction

The first paper of this series (Moro & Munari 2000, Paper I), devoted to the Asiago Database on Photometric Systems (ADPS), presented a compilation of basic information and reference data for ultraviolet, optical and infrared photometric systems, for both the ground-based and space varieties. In Paper I, 167 photometric systems were censed in extenso and other 34 were briefly noted. Only data from the literature were used, with all information traceable back to the original source.

The literature survey in Paper I proved how poorly documented the majority of the systems was and, even when data were provided, it was usually difficult to interpret unambiguously their meaning, or to inter-compare them, because of the highly heterogeneous methods and conventions adopted by different authors. Even basic concepts such as wavelength and width of a band came in so many varieties that common grounds could be established, from literature data, only for a thin minority of the systems (see discussion under *System Description* in Sect. 2 of Paper I). The situation with band and reddening parameters is worth some statistics. Out of 201 censed systems, (*a*) 24% had no wavelength or width information or they were in clear conflict with published band transmission curves, (*b*) 28% had poor information, typically just the mean or peak wavelength, (*c*) 44% had decent information (mainly systems with square bands or interference filters), and only for (*e*) 4% the available information included effective wavelengths for more than one spectral type (just 2% in the case of effective widths). The situation with reddening parameters is even more depressing. Again, out of the 201 censed systems, reddening information was (*i*) completely missing for 78% of them, (*ii*) poorly known for 15% (typically $A(\lambda)/E_{B-V}$ for just one or two bands), (*iii*) satisfactory for 4%, and (*iv*) complete for only 3% of them.

It appears therefore mandatory to establish a common set of parameters for all photometric systems, and to calibrate them via homogeneous synthetic photometry algorithms and a common sample of input spectra. The availability of the same extensive set of homogeneous parameters would support a

Send offprint requests to: U. Munari, e-mail: `munari@pd.astro.it`

⋆ Figures 9–187 are only available in electronic form at the CDS via anonymous ftp to `cdsarc.u-strasbg.fr (130.79.128.5)` or via `http://cdsweb.u-strasbg.fr/cgi-bin/qcat?J/A+A/401/781`

⋆⋆ The source spectra used in the computations are available via the *web* interface to ADPS: `http://ulisse.pd.astro.it/ADPS/`

proper use of the systems, an easier inter-comparison among them and the appreciation of their legacy when attempting the design of a new one.

A first step in such an homogeneous documentation of existing photometric systems is the derivation of band and reddening parameters for all the photometric systems with known transmission curves. The band parameters derived in this paper include various types of wavelengths, widths and moments for a set of normal and peculiar input spectra, as well as polynomial fits of their behavior with blackbody temperature. Reddening parameters include the Cardelli et al. (1989) $a(x)$ and $b(x)$ coefficients, $A(\lambda)/A(V)$ and $A(\lambda)/E_{B-V}$ for various types of source spectra and extinction laws (R_V = 5.0, 3.1 and 2.1), and polynomial fits to the behavior of effective wavelength and width.

All our work is based on synthetic photometry. It is by far the only viable mean to document so many systems on homogeneous grounds. However, it cannot entirely substitute detailed individual characterization of photometric systems based on careful analysis of published observations (when available in large enough number and accuracy). Such individual analysis, by iteratively working on the color differences recorded between known stars, can even lead to a revision of published band profiles (cf. Bessell 2000 revision of the Hipparcos/Tycho band profiles published in the ESA's Hipparcos Catalogue). A detailed characterization based on actual observations has been so far successfully attempted only for very few systems and its application to the >200 censed in the ADPS is vastly out of the scope and possibilities of the present series of papers.

Finally, when compiling Paper I we tried to be as complete as possible for the optical and ultraviolet regions ($\lambda \leq 1\,\mu$m). In the infrared the completeness was known to be lower. To improve the completeness of ADPS, further 12 infrared and additional 5 optical systems are now included, bringing the total number of photometric systems censed by ADPS to 218. The new 17 systems are briefly noted in Sect. 4.

2. Input spectra for synthetic photometry

A set of input spectra for the synthetic photometry to be carried out in this Paper II has been assembled. It includes *normal* and *peculiar* stars. Both sets can be downloaded from the ADPS *web* site, where further information on them is available.

Normal stars include synthetic spectra of ι Her (B3 IV), Vega (A0 V), Sun (G2 V), Arcturus (K2 III) and Betelgeuse (M2 Iab) as representative of the range of stars over the HR diagram. The spectrum of a carbon star characterized by $T_{\rm eff}$ = 3000 K, lg g = 0.0, solar metallicity and C/O = 1.1 is added to the set of normal stars. Vega and the Sun are among the stellar sources more frequently used in literature in the computation of effective wavelengths. The spectrum of ι Her is taken from Castelli et al. (1997), the carbon star spectrum is from Ya. Pavlenko (private communication), and the others were downloaded from Kurucz's web site (`http://kurucz.harvard.edu/`), who computed them. Figure 1 presents the 3000 Å–6 μm portion of these spectra in a linear flux scale and logarithmic wavelength scale.

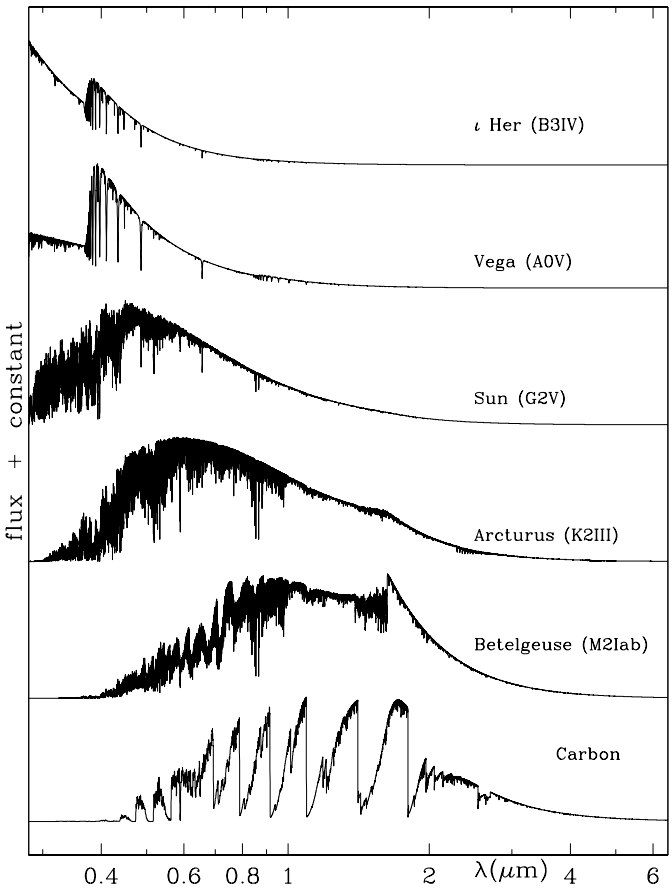

Fig. 1. The set of spectra of *normal* stars used in the computations of this paper.

Peculiar stars include observed spectra of a sample of peculiar objects representative of those affected by emission lines. The spectra, absolutely fluxed, come from the spectral survey of Munari & Zwitter (2002) and cover the wavelength range 3200–9100 Å at a dispersion of ~2.5 Å/pix. The spectra of the *peculiar stars* are used only with the optical photometric systems. For those bands which outer wings extended outside the 3200–9100 Å interval, the spectra of *peculiar stars* have been expanded by blackbody approximations of their continua to cover the whole profile band. Figure 2 displays the spectra in a logarithmic flux scale and linear wavelength scale, suitable to expand the dynamical range of the plot and to emphasize visibility of weak features. The peculiar objects are:

WN: average spectrum of the two Wolf-Rayet stars of nitrogen type HD 50896 and HD 96548;

WC: average spectrum of the two Wolf-Rayet stars of carbon type HD 136488 and HD 165763;

$PN_{\rm Ne}$: spectrum of the compact planetary nebula M1–13, that is given as representative of low electron density conditions (strong forbidden emission lines);

$PN^{\rm Ne}$: spectrum of the compact planetary nebula M1–12, that is given as representative of high electron density conditions (hydrogen emission lines dominating);

Nova: average spectrum of the three novae Nova Lup 1993, Nova Cir 1995 and Nova Cen 1995 during their nebular phases;

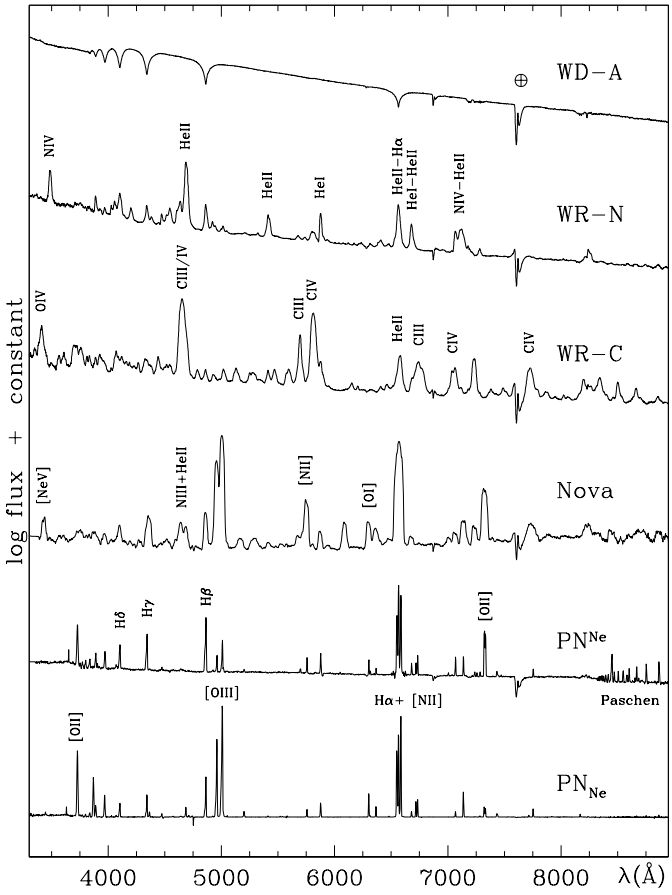

Fig. 2. The set of peculiar spectra used in the computation of equivalent wavelengths and widths. Note the logarithmic scale for the ordinates, used to expand the dynamical range of the plot so to emphasize visibility of weak features. Some guidance to line identification is provided.

WDA: average spectrum of the white dwarfs of type A (hydrogen dominated spectra) EG 274, LTT 7987 and LTT 4816.

3. The database

The database is organized as a series of figures, one for each of the systems with known transmission curves (179 in all). Given their large number, these figures are available in electronic form only, with Fig. 1 given here as an example. Each figure plots in a compressed, normalized format the band transmission profiles (for a finer view and a tabular version see Paper I or the ADPS *web* site), and reports for each band the computed data following the scheme outlined in Fig. 4 and discussed in detail later in this section. Table 1 lists the photometric systems considered in this paper and gives the number of the corresponding figure. The photometric systems are grouped in Table 1 in four distinct categories (ultraviolet, optical, infrared, and mixed systems) because of their slightly different figure layout scheme and input spectra (see detailed description in Sects. 3.1 and 3.2 below). Within each category the chronological order is followed. The names of the photometric systems are the same as used in Paper I. For reader's convenience, the number of the corresponding figure in Paper I is given too.

Actual transmission profiles were presented in Paper I for slightly more than half of the censed systems (105 out of 201). This number is expanded here (179 out of 218) in several ways, and Table 1 summarizes the source for band transmission profiles for all the systems included in this paper. First, transmission profiles have been located in literature for some more systems. Second, transmission profiles have been reconstructed for other systems by combining filter, atmospheric and telescope transmissions with detector response. Details and tabular versions of these new transmission profiles are available via the *web* interface to ADPS. Third, bands that were reported by the authors as obtained with interference filters, but for which the transmission profiles have never been published, are assumed to have a symmetric Gaussian profile. Symmetric Gaussians are generally found to give a satisfactory representation of the actual profiles of interference filters. For example, the *v*, *b*, *y* bands of the *uvby* Hβ *– Strömgren and Crawford – 1956* system[1] (see Fig. 16) are realized with interference filters. If the band and reddening parameters obtained using their actual profiles are compared with those derived using a Gaussian approximation, a mean difference of ~5.1 Å (~0.1%) is found for the various types of wavelengths and 3.9 Å (~2.0%) for the equivalent widths. Similar figures are obtained for interference filters of other photometric systems. It may be than assumed that approximating with symmetric Gaussians the unknown transmission profiles of bands realized with interference filters is an acceptable procedure, suitable to provide results accurate to better than 5% for band wavelengths and better than 10% for band widths. For those interference filters that are particularly wide, the accuracy could be lower.

The data contained in Fig. 3 (and those of the other ones available in electronic form only) are described in the subsections below, following the scheme numbered in Fig. 4. The band parameters (areas ❶ ❷ ❸ and ❹) are discussed first, followed by the reddening parameters (areas ❺ ❻ ❼ ❽ and ❾). In this paper $F(\lambda)$ is the transmission profile of the band, $f(\lambda)$ the same normalized to 1.0 at its maximum, $S(\lambda)$ the energy distribution of a source spectrum and $\mathcal{B}(T,\lambda)$ the Planck function for the temperature T. In the figures, quantities for ultraviolet and optical systems are expressed in Å, in μm for the infrared ones.

3.1. Data scheme for band parameters

3.1.1. Area ❶

The information contained within this area pertains to the pure band transmission profile, without convolution with a source spectrum. Figure 5 provides a graphical representation for some of the quantities here considered.

[1] The naming of the systems is that introduced and explained in Paper I. In this case it follows from Strömgren (1956, 1963, 1966), Crawford (1958, 1960), Crawford & Mander (1966), and Crawford & Barnes (1970). The system name thus summarizes the symbols for the bands, the names of the principal authors, and the year it was first introduced.

Table 1. List of the 179 photometric systems considered in this paper (all those with known transmission curves among the 218 so far censed by the ADPS project). The names of the systems are the same as in Paper I. Columns 4–6 give respectively the number of the electronic figure devoted to the given system, the number of photometric bands considered in this paper and the type of source for their transmission profiles, while Col. 7 lists the number of the corresponding figure in Paper I (*bn*: systems only briefly noted in Paper I, Sect. 3). The sources for the transmission profiles are coded as follow. *Tabular*: as tabulated by the author(s); *graph*: derived by us from plots of the transmission profiles published by the author(s); *rectangl*: rectangular profiles as prescribed by the author(s); *reconstr*: reconstructed for this paper by combining the detector sensitivity with filter and atmospheric transmission; *Gaussian*: a Gaussian profile is assumed for the narrow bands obtained with interference filters and for which no other information is available.

			ADPS 2			ADPS 1
system	**year**	**authors**	**fig.**	**bands**	**res.**	**fig.**
		optical systems				
UVBGRI	1943	Stebbins and Whitford	9	6	tabular	2
RGU	1946	Becker	10	3	tabular	3
RI	1951	Kron and Smith	11	3	graph	4
UBV	1953	Johnson and Morgan	12 a-d	15	tabular	6
POSS I	1955		13	3	tabular	7
PV	1955	Eggen	14	3	tabular	8
	1955	Strömgren and Gyldenkerne	15	5	gaussian	
*uvbyH*β	1956	Strömgren and Crawford	16	6	graph	10
U_cBV	1958	Arp	17	3	tabular	12
ubgyri	1958	Bahng	18	6	tabular	13
UV BG R	1958	Tifft	19	6	tabular	14
5 colors	1959	Borgman	20	5	graph	15
KLMNPQR	1960	Borgman	21 a,b	7	tabular	16
	1960	Deeming	22	3	rectangl	17
	1960	Griffin and Redman	23	6	rectangl	19
	1960	Kraft	24	2	gaussian	*bn*
USNO	1960	Kron and Mayall	25	3	reconstr	20
VBLUW	1960	Walraven and Walraven	26	5	tabular	21
	1961	Griffin	27	6	rectangl	22
8 colors	1961	Tifft	28 a,b	8	tabular	23
*H*γ	1962	Bappu *et al.*	29	3	gaussian	24
Geneva	1962	Golay	30 a,b	7	tabular	25
	1963	Bahner	31 a-c	16	rectangl	
$ubvr_{20}$	1963	Sandage and Smith	32	4	tabular	26
	1964	Barbier and Morguleff	33 a,b	8	rectangl	27
*H*γ	1964	Beer	34	3	rectangl	28
*H*α	1964	Peat	35	3	rectangl	29
*H*α,β,γ,δ	1965	Abt and Golson	36 a,b	8	gaussian	31
	1965	Miner	37 a,b	7	gaussian	34
Vilnius	1965	Straižys *et al.*	38 a,b	8	tabular	35
UVBY	1966	Kruszewski	39	4	tabular	36
4 colors	1966	Neff and Travis	40	4	tabular	37
	1966	Scarfe	41 a-d	22	rectangl	38
ubVt	1966	Smak	42	5	graph	39
ubvr	1966	Westerlund	43	4	gaussian	40
12 colors	1966	Wood	44 a,b	12	tabular	41
ri	1967	Argue	45	4	graph	42
	1967	Boyce	46	6	rectangl	43
62 65 102	1967	Eggen	47	3	tabular	44
LPL	1967	Johnson *et al.*	48 a,b	8	tabular	45
27 colors	1967	Wing	49 a,b	9	rectangl	46
Hα	1968	Andrews	50	6	rectangl	47
DDO	1968	McClure and Van den Bergh	51 a-c	13	tabular	48
*H*β,γ	1968	Sinnerstad *et al.*	52 a,b	11	graph	49
u'ubvv'	1968	Smith	53	5	gaussian	50
Ca II K	1969	Henry	54	2	rectangl	52
	1969	Newell *et al.*	55	4	graph	53
	1969	Spinrad and Taylor	56 a-f	33	rectangl	54
*H*α,β	1969	Tebbe	57	4	gaussian	55
gnkmfu	1970	Dickow *et al.*	58 a,b	8	gaussian	56
Uppsala	1970	Häggkvist and Oja	59	3	gaussian	57
RI	1970	Jacobsen	60	2	graph	58
nh	1970	Landolt	61	4	gaussian	59
	1970	McNamara *et al.*	62	3	gaussian	*bn*
	1970	Morguleff *et al.*	63 a,b	11	rectangl	60
Hγ	1971	Häggkvist	64	3	gaussian	62
DAO	1971	Hill *et al.*	65	6	rectangl	63

Table 1. continued.

			ADPS 2			ADPS 1
system	**year**	**authors**	**fig.**	**bands**	**res.**	**fig.**
5 colors	1971	Lockwood and Wing	66	5	gaussian	64
	1971	Mendoza	67	3	graph	65
	1971	Wawrukiewicz	68	4	gaussian	*bn*
	1971	Williams *et al.*	69 a,b	9	rectangl	66
8 colors	1971	Wing	70 a,b	10	gaussian	67
	1972	Jones and Dixon	71	4	gaussian	69
	1972	Lutz and Lutz	72	2	gaussian	*bn*
*H*α,β	1972	Peton *et al.*	73	5	graph	70
	1972	Seeds	74	4	gaussian	*bn*
$u_A b_A \beta_A y_A$	1972	Wickramasinghe and Strittmatter	75	4	gaussian	71
	1973	Caplan	76	2	rectangl	*bn*
24 colors	1973	Chapman *et al.*	77 a-d	24	gaussian	73
	1973	Cherepashchuk and Khaliullin	78	5	gaussian	*bn*
10 colors	1973	Faber	79 a,b	10	graph	74
	1973	Jones and Carrick	80	6	rectangl	*bn*
WBVR	1973	Straižys	81	4	tabular	76
	1974	Alexander and Branch	82	3	gaussian	78
UBVR	1974	Cathey	83	4	reconstr	79
	1974	Faÿ *et al.*	84	5	rectangl	*bn*
*H*α,β,γ	1974	Feinstein	85 a,b	10	gaussian	80
UBVRI	1974	Fernie	86	5	reconstr	81
*H*α,β	1974	Guinan and McCook	87	4	gaussian	82
	1974	Sorvari	88	2	gaussian	*bn*
Hα	1974	Vidal	89	2	reconstr	84
Hα	1975	Dachs and Schmidt-Kaler	90	2	gaussian	86
	1975	Helt and Gyldenkerne	91 a,b	9	gaussian	87
8 colors	1975	Morguleff *et al.*	92 a,b	8	rectangl	89
ri	1975	Weistrop	93	2	reconstr	90
Washington	1976	Canterna	94 a,b	8	tabular	92
RI	1976	Cousins	95	2	tabular	93
	1976	Greenstein	96 a,b	8	rectangl	*bn*
13 colors	1976	Johnson and Mitchell	97 a-c	14	tabular	95
$vbyg_1g_2$	1976	Maitzen	98	2	graph	96
	1976	Mould	99 a,b	7	rectangl	*bn*
uvgr	1976	Thuan and Gunn	100	4	graph	97
Trieste	1977	Cester *et al.*	101	2	graph	99
	1977	Dzervitis	102	6	gaussian	*bn*
	1977	Mould and Wallis	103	5	gaussian	
	1978	Mould and McElroy	104	4	gaussian	*bn*
ubVr	1978	Sandage and Visvanathan	105	6	gaussian	101
8 colors	1978	White and Wing	106 a,b	8	gaussian	102
U'JF	1979	van der Kruit	107	3	graph	103
$B_J R_F$	1980	Couch and Newell	108	4	tabular	106
$uvgr\ 39_B\ 39_N$	1980	Zinn	109	2	gaussian	108
	1981	Avetisyan *et al.*	110 a,b	7	gaussian	*bn*
Δ*a*	1981	Joncas and Borra	111	3	graph	110
	1981	Jones *et al.*	112	4	tabular	111
*H*α	1981	Strauss and Ducati	113	2	gaussian	112
VilGen	1982	North *et al.*	114 a,b	7	graph	115
	1982	Solheim *et al.*	115 a,b	10	graph	116
8 colors	1982	Tedesco *et al.*	116 a,b	8	graph	117
UBVRI	1983	Landolt	117	5	reconstr	119
griz	1983	Schneider *et al.*	118	4	graph	120
RGU	1983	Trefzger *et al.*	119	3	tabular	121
	1984	Hartwick *et al.*	120	4	rectangl	*bn*
	1984	Nersisian	121 a,b	9	gaussian	*bn*
WBVR	1985	Khaliullin *et al.*	122	4	tabular	125
	1986	Park and Lee	123	4	reconstr	127
	1987	Herbst *et al.*	124	3	graph	*bn*
	1987	Kenyon and Fernandez-Castro	125 a,b	10	rectangl	128
ψ(25)	1987	Mendoza	126	3	graph	129
	1988	Faulkner *et al.*	127	6	gaussian	*bn*
77 81	1989	Cook and Aaronson	128	2	gaussian	131
$g_4r_4i_4z_4$	1989	Schneider *et al.*	129	4	graph	132
Hipparcos	1989		130 a,b	6	tabular	135

Table 1. continued.

system	year	authors	ADPS 2 fig.	ADPS 2 bands	ADPS 2 res.	ADPS 1 fig.
UBVRI	1990	Bessell	131	6	tabular	136
Guide Star Catalogue	1990	Lasker *et al.*	132	4	reconstr	138
POSS II	1991	Reid *et al.*	133	3	graph	141
CaII	1991	Twarog *et al.*	134	2	tabular	142
20 colors	1992	Bastiaansen	135 a-d	20	graph	143
MACHO	1992		136	2	tabular	144
FPBS	1995	Brewer *et al.*	137	2	gaussian	151
BATC	1996	Fan *et al.*	138 a-c	16	tabular	153
Sloan DSS	1996	Fukugita *el al.*	139	5	tabular	154
StrömVil	1996	Straižys *et al.*	140 a,b	7	tabular	155
	1997	Damineli *et al.*	141	3	graph	159
	1997	Malyuto *et al.*	142 a-c	18	rectangl	
TNG	1997	Marchetti *et al.*	143 a,b	8	graph	160
UWTAT	1997	Strassmeier *et al.*	144 a-c	13	graph	162
	1998	Hickson and Mulrooney	145 a-f	33	graph	
	1998	Royer *et al.*	146	5	gaussian	165
Asiago GAIA	1998	Munari	147 a-c	14	tabular	166
Geneva GAIA	1999	Grenon *et al.*	148 a-c	14	tabular	167
	1999	Vansevičius *et al.*	149	2	rectangl	*bn*
ultraviolet systems						
Aerobee UV-55	1955		150	1	graph	9
OAO2 WEP	1970		151 a,b	12	tabular	61
TD1	1972		152 a-e	25	rectangl	72
ANS	1974		153	6	graph	85
D2B AURA	1975		154	4	rectangl	91
VWFSC Spacelab 1	1983		155	3	graph	123
UIT	1990		156 a,b	11	graph	139
infrared systems						
JHKL SAAO	1973	Glass	157 a,b	7	graph	75
	1973	Khozof *et al.*	158	3	gaussian	*bn*
NQ	1974	Low and Rieke	159	2	graph	83
JHK H_2O *CO*	1977	Persson *et al.*	160	3	graph	100
	1978	Pilachowski	161	2	gaussian	*bn*
JHK KPNO	1979	Manduca and Bell	162	3	graph	
KAO far-IR	1979	Harvey	163	5	graph	
	1982	Avetisyan and Melik-Alaverdyan	164 a,b	10	gaussian	*bn*
JHKL MSO	1982	Jones and Hyland	165	3	graph	114
IRAS	1983		166	4	tabular	122
	1984	McWilliam and Lambert	167	2	graph	*bn*
$J_nK_nL_nM_n$	1986	Leggett *et al.*	168	4	graph	126
VJHKLL'M	1988	Bessell and Brett	169	6	tabular	130
SCAS	1993	Clark *et al.*	170 a,b	7	graph	145
JHKL' CST	1994	Alonso *et al.*	171	4	tabular	147
DENIS	1994	Epchtein *et al.*	172	3	graph	148
IRTS FIRP	1994	Lange *et al.*	173	4	graph	
S-520-15 FIR	1994	Matsuhara *et al.*	174	5	graph	
JHKL MSSSO	1994	McGregor	175	4	graph	149
IRTF NSFCAM	1994	Shure *et al.*	176 a-c	18	tabular	150
iz,iJ,iH,iK,iL,iL',iM,in,iN,iQ	1994	Young *et al.*	177 a,b	10	tabular	
ISOCAM ISO	1995		178 a-d	21	tabular	152
ESO NIR	1996	Van der Bliek *et al.*	179	5	gaussian	157
NICMOS HST	1997		180 a-f	32	tabular	163
ABU SPIREX	1998		181	6	tabular	
JHK'K_S*KL'M'* MKO	2002	Tokunaga *et al.*	182 a,b	7	tabular	
mixed systems						
UBVRI(JHKLMN)	1965	Johnson	183 a-c	11	tabular	33
FOC HST	1989		184 a-h	39	tabular	133
WFPC1 HST	1989		185 a-g	37	tabular	134
WFPC2 HST	1993		186 a-f	36	tabular	146
STIS HST	1997		187 a-c	15	tabular	164

Sloan DSS - Fukugita et al. - 1996

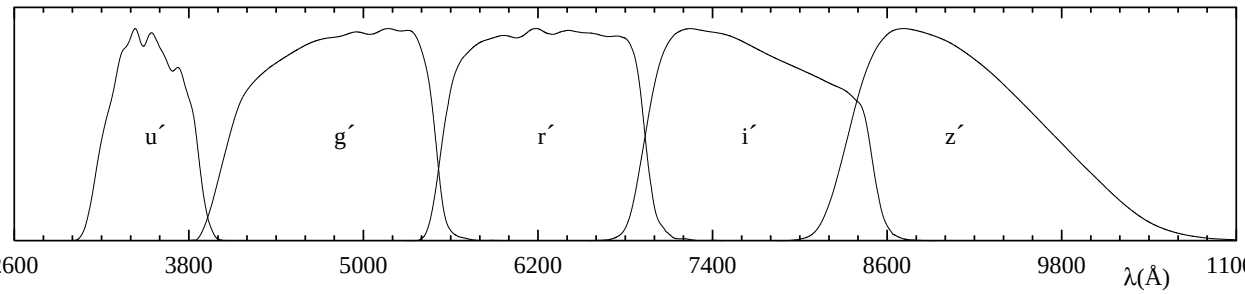

u′

				B3	*Vega*	*Sun*	*K2*	*M2*	*Carbon*
$\lambda_c = 3530$	$\lambda_\circ = 3521$	$\lambda_{peak} = 3431$	$\lambda_{gauss} = 3519$	3504	3551	3538	3593	3636	3525
WHM = 642	W10% = 831	W80% = 437	FWHM = 555	[599]	[602]	[565]	[517]	[448]	[498]
$W_\circ = 590$	$\frac{A(\lambda)}{A(V)}\|_{5.0} = 1.36\,^{1.34}_{1.40}$	$a = {}^{0.934}_{0.944}$ $b = {}^{2.036}_{1.972}$	*B3*	*WN*	*WC*	PN_{Ne}	PN^{Ne}	*Nova*	*WDA*
$\mu = 201$	$\frac{A(\lambda)}{A(V)}\|_{3.1} = 1.61\,^{1.58}_{1.69}$	$a = {}^{0.942}_{0.949}$ $b = {}^{1.985}_{1.934}$	*Sun*	3489	3500	3642	3533	3517	3481
$I_{asym} = 0.01$	$\frac{A(\lambda)}{A(V)}\|_{2.1} = 1.95\,^{1.88}_{2.08}$	$\frac{A(\lambda)}{E(B-V)}$: $(4.946, 0.067)^{r=0.99}_{B3}$		$(5.271, 0.091)^{r=1.00}_{Sun}$		$(5.888, 0.075)^{r=1.00}_{M2}$			
$I_{kurt} = -0.88$	$\lambda_{eff} = 3521.5 + 41.9 \times E(B-V)$ r=1.00			$W_{eff} = 600.1 - 38.8 \times E(B-V)$ r=–0.98					
	$\lambda_{eff}(T) = 3472 + 145 \times \theta + 77 \times \theta^2 - 55 \times \theta^3$			$W_{eff}(T) = 556 + 263 \times \theta - 562 \times \theta^2 + 193 \times \theta^3$					

g′

				B3	*Vega*	*Sun*	*K2*	*M2*	*Carbon*
$\lambda_c = 4788$	$\lambda_\circ = 4803$	$\lambda_{peak} = 5173$	$\lambda_{gauss} = 4820$	4683	4708	4817	4903	5015	5100
WHM = 1411	W10% = 1641	W80% = 1111	FWHM = 1245	[1238]	[1271]	[1318]	[1230]	[1057]	[1004]
$W_\circ = 1325$	$\frac{A(\lambda)}{A(V)}\|_{5.0} = 1.12\,^{1.10}_{1.13}$	$a = {}^{1.011}_{1.015}$ $b = {}^{0.656}_{0.486}$	*B3*	*WN*	*WC*	PN_{Ne}	PN^{Ne}	*Nova*	*WDA*
$\mu = 419$	$\frac{A(\lambda)}{A(V)}\|_{3.1} = 1.19\,^{1.16}_{1.20}$	$a = {}^{1.015}_{1.016}$ $b = {}^{0.507}_{0.371}$	*Sun*	4696	4706	4943	4767	4923	4716
$I_{asym} = -0.12$	$\frac{A(\lambda)}{A(V)}\|_{2.1} = 1.28\,^{1.24}_{1.30}$	$\frac{A(\lambda)}{E(B-V)}$: $(3.804, -0.006)^{r=-0.78}_{B3}$		$(3.949, 0.009)^{r=0.95}_{Sun}$		$(4.281, -0.000)^{r=-0.08}_{M2}$			
$I_{kurt} = -1.04$	$\lambda_{eff} = 4807.4 + 142.3 \times E(B-V)$ r=1.00			$W_{eff} = 1371.8 - 208.0 \times E(B-V)$ r=–0.99					
	$\lambda_{eff}(T) = 4647 + 312 \times \theta + 241 \times \theta^2 - 173 \times \theta^3$			$W_{eff}(T) = 1156 + 909 \times \theta - 1424 \times \theta^2 + 387 \times \theta^3$					

r′

				B3	*Vega*	*Sun*	*K2*	*M2*	*Carbon*
$\lambda_c = 6242$	$\lambda_\circ = 6253$	$\lambda_{peak} = 6191$	$\lambda_{gauss} = 6247$	6160	6168	6220	6256	6307	6365
WHM = 1387	W10% = 1565	W80% = 1248	FWHM = 1262	[1282]	[1294]	[1335]	[1341]	[1315]	[1251]
$W_\circ = 1343$	$\frac{A(\lambda)}{A(V)}\|_{5.0} = 0.88\,^{0.88}_{0.89}$	$a = {}^{0.947}_{0.938}$ $b = {}^{-0.205}_{-0.224}$	*B3*	*WN*	*WC*	PN_{Ne}	PN^{Ne}	*Nova*	*WDA*
$\mu = 407$	$\frac{A(\lambda)}{A(V)}\|_{3.1} = 0.83\,^{0.84}_{0.85}$	$a = {}^{0.941}_{0.933}$ $b = {}^{-0.218}_{-0.235}$	*Sun*	6220	6124	6531	6432	6444	6156
$I_{asym} = -0.01$	$\frac{A(\lambda)}{A(V)}\|_{2.1} = 0.77\,^{0.77}_{0.79}$	$\frac{A(\lambda)}{E(B-V)}$: $(2.615, 0.020)^{r=0.99}_{B3}$		$(2.770, 0.028)^{r=1.00}_{Sun}$		$(3.099, 0.013)^{r=0.98}_{M2}$			
$I_{kurt} = -1.09$	$\lambda_{eff} = 6253.4 + 91.0 \times E(B-V)$ r=1.00			$W_{eff} = 1370.2 - 106.1 \times E(B-V)$ r=–0.98					
	$\lambda_{eff}(T) = 6145 + 139 \times \theta + 156 \times \theta^2 - 80 \times \theta^3$			$W_{eff}(T) = 1255 + 289 \times \theta - 183 \times \theta^2 - 109 \times \theta^3$					

i′

				B3	*Vega*	*Sun*	*K2*	*M2*	*Carbon*
$\lambda_c = 7704$	$\lambda_\circ = 7667$	$\lambda_{peak} = 7242$	$\lambda_{gauss} = 7635$	7573	7584	7620	7649	7732	7653
WHM = 1532	W10% = 1756	W80% = 1005	FWHM = 1291	[1322]	[1335]	[1359]	[1369]	[1340]	[1453]
$W_\circ = 1374$	$\frac{A(\lambda)}{A(V)}\|_{5.0} = 0.66\,^{0.66}_{0.68}$	$a = {}^{0.818}_{0.812}$ $b = {}^{-0.487}_{-0.503}$	*B3*	*WN*	*WC*	PN_{Ne}	PN^{Ne}	*Nova*	*WDA*
$\mu = 453$	$\frac{A(\lambda)}{A(V)}\|_{3.1} = 0.61\,^{0.61}_{0.64}$	$a = {}^{0.814}_{0.808}$ $b = {}^{-0.497}_{-0.513}$	*Sun*	7582	7625	7495	7608	7623	7582
$I_{asym} = 0.14$	$\frac{A(\lambda)}{A(V)}\|_{2.1} = 0.54\,^{0.54}_{0.58}$	$\frac{A(\lambda)}{E(B-V)}$: $(1.906, 0.020)^{r=0.99}_{B3}$		$(2.028, 0.026)^{r=1.00}_{Sun}$		$(2.260, 0.016)^{r=0.99}_{M2}$			
$I_{kurt} = -1.05$	$\lambda_{eff} = 7666.9 + 78.9 \times E(B-V)$ r=1.00			$W_{eff} = 1391.2 - 65.7 \times E(B-V)$ r=–0.97					
	$\lambda_{eff}(T) = 7562 + 101 \times \theta + 123 \times \theta^2 - 52 \times \theta^3$			$W_{eff}(T) = 1310 + 144 \times \theta - 9 \times \theta^2 - 104 \times \theta^3$					

z′

				B3	*Vega*	*Sun*	*K2*	*M2*	*Carbon*
$\lambda_c = 9038$	$\lambda_\circ = 9115$	$\lambda_{peak} = 8717$	$\lambda_{gauss} = 9018$	9022	9046	9057	9086	9136	9076
WHM = 1408	W10% = 2212	W80% = 845	FWHM = 1326	[1379]	[1390]	[1400]	[1412]	[1410]	[1562]
$W_\circ = 1411$	$\frac{A(\lambda)}{A(V)}\|_{5.0} = 0.48\,^{0.48}_{0.50}$	$a = {}^{0.677}_{0.670}$ $b = {}^{-0.622}_{-0.613}$	*B3*	*WN*	*WC*	PN_{Ne}	PN^{Ne}	*Nova*	*WDA*
$\mu = 536$	$\frac{A(\lambda)}{A(V)}\|_{3.1} = 0.45\,^{0.45}_{0.48}$	$a = {}^{0.673}_{0.665}$ $b = {}^{-0.617}_{-0.611}$	*Sun*	9027	9016	8894	9022	9068	8993
$I_{asym} = 0.48$	$\frac{A(\lambda)}{A(V)}\|_{2.1} = 0.42\,^{0.41}_{0.45}$	$\frac{A(\lambda)}{E(B-V)}$: $(1.417, 0.018)^{r=0.99}_{B3}$		$(1.512, 0.023)^{r=1.00}_{Sun}$		$(1.702, 0.015)^{r=0.99}_{M2}$			
$I_{kurt} = -0.39$	$\lambda_{eff} = 9113.4 + 73.5 \times E(B-V)$ r=1.00			$W_{eff} = 1422.0 - 42.8 \times E(B-V)$ r=–0.97					
	$\lambda_{eff}(T) = 8997 + 88 \times \theta + 105 \times \theta^2 - 36 \times \theta^3$			$W_{eff}(T) = 1357 + 91 \times \theta + 24 \times \theta^2 - 76 \times \theta^3$					

Fig. 3. The figure relative to the *Sloan DSS – Fukugita et al. – 1996* photometric system is presented as an example of Figs. 9–187 only available in electronic form at the CDS.

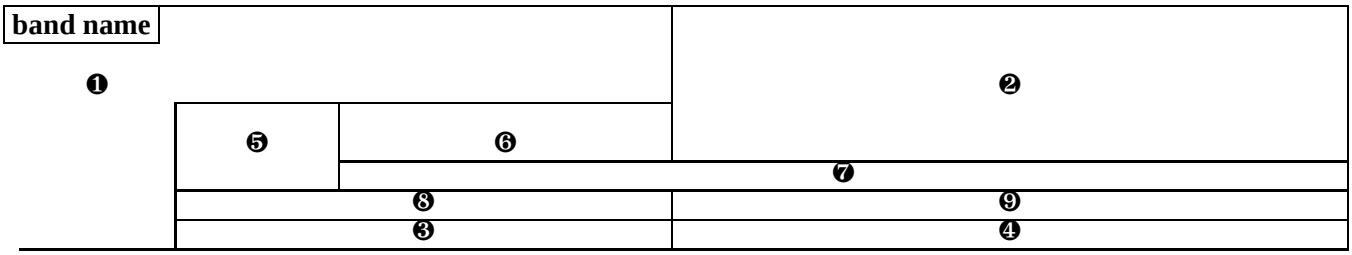

Fig. 4. Scheme for the organization of numerical data in the figures devoted to the documentation of the photometric systems (see also Fig. 3). The *areas* in which data are organized are labelled in the same order as they are described in the text in Sects. 3.1.1 to 3.2.5.

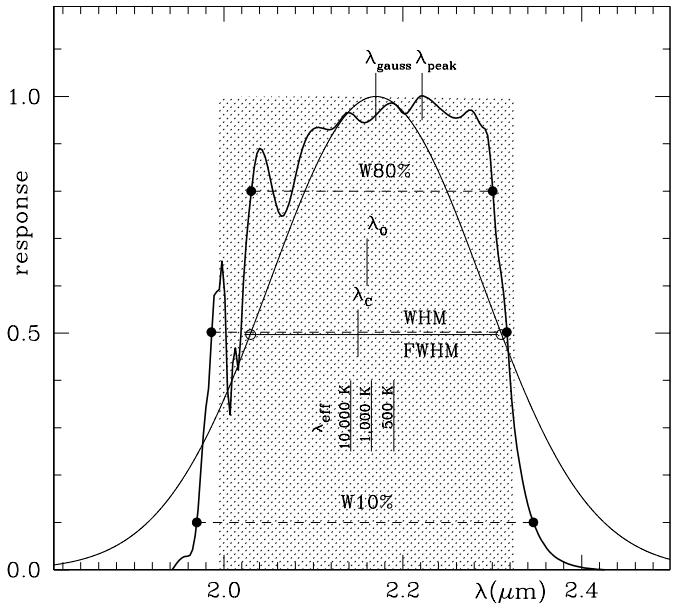

Fig. 5. Graphical representation of some of the wavelength and width quantities described in Sects. 3.1.1 and 3.1.2. The band is K_s from the *DENIS – Epchtein et al. – 1994* system (cf. Fig. 172). The shadowed area is the band equivalent width $W_\circ$.

λ_c is the wavelength halfway between the points where the band transmission profile reaches half of the maximum value. In some cases the bands have complicated shapes, with the band transmission profile crossing several times the 50%-line, like the *N* band of the *NQ – Low and Rieke – 1974* system in Fig. 159. In all such cases the most external 50% points are taken in computing λ_c.

$\lambda_\circ$ is the mean wavelength of the band:

$$\lambda_\circ = \frac{\int \lambda\, F(\lambda)\, \mathrm{d}\lambda}{\int F(\lambda)\, \mathrm{d}\lambda}. \qquad (1)$$

λ_{peak} is the wavelength at which the band transmission profile reaches its maximum.

λ_{gauss} is the central wavelength of the approximating Gaussian with an area equal to that of the actual band transmission profile. If both the band and the Gaussian are normalized to 1.0 at peak response, and $\mathcal{A}$ is the area of the band, the equal-area fitting Gaussian is then:

$$g(\lambda) = \exp\left[-\pi \frac{(\lambda - \lambda_{\mathrm{gauss}})^2}{\mathcal{A}^2}\right]. \qquad (2)$$

The value of λ_{gauss} has been computed using the Levenberg-Marquardt method (Press et al. 1988).

WHM is the the full wavelength span between the points where the band transmission profile reaches half of the maximum value. As for λ_c, in the case of complicated band profiles the most external 50% points are taken when computing *WHM*.

*W*10% is the wavelength span between the points where the band transmission profile reaches 10% of the maximum value. In the case of complicated band profiles the most external 10% points are taken in computing W10%. It is worth noticing that for a Gaussian profile of area $\mathcal{A}$, dispersion σ and 1.00 peak transmission it is:

$$W10\% = 2\mathcal{A}\sqrt{(\ln 10)/\pi} = 1.712\,\mathcal{A} = 2\sigma\sqrt{2\ln 10} = 4.292\,\sigma. \qquad (3)$$

*W*80% is the wavelength span between the points where the band transmission profile reaches 80% of the maximum value. Again, in the case of complicated band profiles, the most external 80% points are taken in computing W80%. It is worth noticing that for a Gaussian profile of area $\mathcal{A}$, dispersion σ and 1.00 peak transmission it is:

$$W80\% = 2\mathcal{A}\sqrt{(\ln 1.25)/\pi} = 0.533\,\mathcal{A} = 2\sigma\sqrt{2\ln 1.25} = 1.336\,\sigma. \qquad (4)$$

FWHM is the full width at half maximum of the approximating Gaussian with an area equal to that of the actual band transmission profile. If both the band and the Gaussian are normalized to 1.0 at peak response, and $\mathcal{A}$ is the area of the band, then:

$$FWHM = 2\mathcal{A}\sqrt{(\ln 2)/\pi} = 0.939\,\mathcal{A} = 2\sigma\sqrt{2\ln 2} = 2.355\,\sigma. \qquad (5)$$

$W_\circ$ is the equivalent width of the band transmission profile:

$$W_\circ = \int f(\lambda)\, \mathrm{d}\lambda = \frac{1}{C}\int F(\lambda)\, \mathrm{d}\lambda \qquad (6)$$

where $C = [F(\lambda)/f(\lambda)]$ is the normalization factor. $W_\circ$ is the area shadowed in Fig. 5.

$\boxed{\mu}$ is the 2nd order momentum of the band transmission profile (for a discussion see Golay 1974, pp. 41–43), i.e. the square root of the expression:

$$\mu^2 = \frac{\int(\lambda - \lambda_\circ)^2 F(\lambda)\,\mathrm{d}\lambda}{\int F(\lambda)\,\mathrm{d}\lambda}. \quad (7)$$

For a Gaussian profile it is $\mu = \sigma$, while for a rectangular band of width W it is $\mu = \sqrt{3}/6\ W$.

$\boxed{I_{\rm asym}}$ is the *skewness* index and it closely resembles the 3rd order moment (the only difference lies in the presence of μ^3):

$$I_{\rm asym} = \frac{\int(\lambda - \lambda_\circ)^3 F(\lambda)\,\mathrm{d}\lambda}{\mu^3 \int F(\lambda)\,\mathrm{d}\lambda} \quad (8)$$

with μ being given by Eq. (7). An $I_{\rm asym} < 0.0$ pertains to a band with an extended blue wing (as the band *i* of the *ri – Argue – 1967* system in Fig. 45 that has $I_{\rm asym} = -1.32$), and $I_{\rm asym} > 0.0$ to a band with an extended red wing (as the band *R* of the *WBVR – Straižys – 1973* system in Fig. 81 that has $I_{\rm asym} = +0.66$). Symmetric profiles are characterized by $I_{\rm asym} = 0.0$ (as the band *35* of the system *DDO – McClure and Van den Bergh – 1968* in Fig. 51a for which it is $I_{\rm asym} = 0.06$).

$\boxed{I_{\rm kurt}}$ is the *kurtosis* index and it closely resembles the 4rd order moment (the only difference lies in the presence of μ^4. For the normalization constant −3 see below):

$$I_{\rm kurt} = \frac{\int(\lambda - \lambda_0)^4 F(\lambda)\,\mathrm{d}\lambda}{\mu^4 \int F(\lambda)\,\mathrm{d}\lambda} - 3. \quad (9)$$

The kurtosis index gives an indication of the balance between the core and the wings of a profile. The −3 is inserted to have $I_{\rm kurt} = 0.0$ for a Gaussian profile. A $I_{\rm kurt} > 0.0$ indicates a band transmission profile more sharply peaked than a Gaussian, i.e. with more wings than core (as the band *P* for the *KLMNPQR – Borgman – 1960* system in Fig. 21a that has $I_{\rm kurt} = +1.66$). A $I_{\rm kurt} < 0.0$ pertains instead to a band with more core than wings (as the band T_2 for the photoelectric version of the *Washington – Canterna – 1976* system in Fig. 94a that has $I_{\rm kurt} = -1.08$). The kurtosis index for a rectangular band is $I_{\rm kurt} = -6/5$, for an equilateral triangular band it is $I_{\rm kurt} = -3/5$, and for an $e^{-|x|}$ profile it is $I_{\rm kurt} = 3$.

Figure 6 provides a graphical representation of μ, $I_{\rm asym}$ and $I_{\rm kurt}$ for some reference profiles.

Several systems contain rectangular or Gaussian bands. In the corresponding figures only non-redundant data are provided. It is therefore appropriate to summarize here for these two types of profiles the values of the above described parameters. For a rectangular band with 1.00 peak transmission and width W it is:

$$\lambda_c \equiv \lambda_\circ \equiv \lambda_{\rm peak} \equiv \lambda_{\rm gauss} \quad (10)$$

$$WHM \equiv W10\% \equiv W80\% \equiv W \equiv W_\circ \quad (11)$$

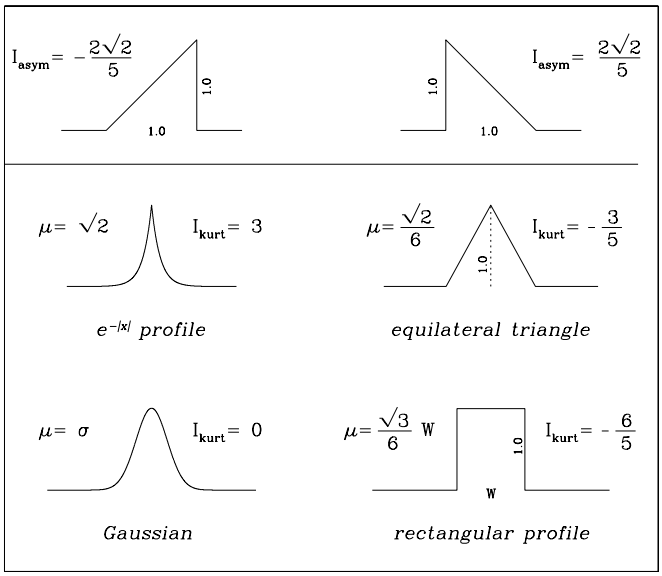

Fig. 6. Values of the 2nd order moment (μ), the skewness and the kurtosis indices for some sample profiles.

$$FWHM = 2W_\circ\sqrt{(\ln 2)/\pi} = 0.939\ W_\circ \quad (12)$$

$$\mu = \sqrt{3}/6\ W_\circ = 0.289\ W_\circ \quad (13)$$

$$I_{\rm asym} = 0 \quad (14)$$

$$I_{\rm kurt} = -\frac{6}{5} \quad (15)$$

and for a Gaussian profiles of peak transmission 1.00 it is:

$$\lambda_c \equiv \lambda_\circ \equiv \lambda_{\rm peak} \equiv \lambda_{\rm gauss} \quad (16)$$

$$W_\circ = \frac{1}{2}\sqrt{\pi/\ln 2}\ FWHM = 1.064\ FWHM \quad (17)$$

$$W10\% = \sqrt{\frac{\ln 10}{\ln 2}}FWHM = 1.823\ FWHM \quad (18)$$

$$W80\% = \sqrt{\frac{\ln 1.25}{\ln 2}}FWHM = 0.567\ FWHM \quad (19)$$

$$FWHM = WHM \quad (20)$$

$$\mu = \sigma = 0.425\ FWHM \quad (21)$$

$$I_{\rm asym} = 0 \quad (22)$$

$$I_{\rm kurt} = 0. \quad (23)$$

3.1.2. Area ❷

This area documents how effective wavelengths (upper rows) and widths (in square bracketts) change with the source spectra $S(\lambda)$ described in Sect. 2. The effective wavelength is:

$$\lambda_{\rm eff} = \frac{\int \lambda\, F(\lambda)\, S(\lambda)\,\mathrm{d}\lambda}{\int F(\lambda)\, S(\lambda)\,\mathrm{d}\lambda}. \quad (24)$$

The effective width $W_{\rm eff}$ is the width of a rectangular bandpass of height 1.0, centered at $\lambda_{\rm eff}$, that collects from a source $S(\lambda)$ the same amount of energy going through the filter $f(\lambda)$:

$$\int f(\lambda)\, S(\lambda)\,\mathrm{d}\lambda = \int_{\lambda_{\rm eff}-W_{\rm eff}/2}^{\lambda_{\rm eff}+W_{\rm eff}/2} S(\lambda)\,\mathrm{d}\lambda \quad (25)$$

$W_{\rm eff}$ is the amount by which to multiply the flux per unit wavelength (normally expressed, for example, is erg cm^2 s^{-1} Å^{-1} at $\lambda_{\rm eff}$) to obtain the flux through the whole band (normally expressed, for example, in erg cm^2 s^{-1}).

Different data schemes are adopted for optical, ultraviolet and infrared systems:

optical systems. All *normal* and *peculiar* spectra discussed in Sect. 2 are considered. For normal spectra, both the effective wavelength and width are given, while for peculiar spectra only the effective wavelength is listed;

ultraviolet systems. For UV systems the effective wavelength and width are computed for the Sun ($T_{\rm eff}$ = 5770 K), Vega ($T_{\rm eff}$ = 9550 K) and ι Her ($T_{\rm eff}$ = 17 100 K), and for three Kurucz's models completing the sequence toward higher temperatures: $T_{\rm eff}$ = 20 000, 30 000 and 40 000 with $[Z/Z_\odot] = 0.0$ and $\lg g = 5.0$;

near-IR systems. For bands between 1 and 8 μm the effective wavelength and width are computed for the same set of *normal* stars used with optical photometric systems;

far-IR systems. For bands longward of 8 μm the effective wavelength and effective width are computed for blackbody energy distributions characterized by the temperatures $T_{\rm eff}$ = 3000, 1500, 800, 400, 200 and 100 K.

3.1.3. Area ❸

The effective wavelength of a blackbody energy distribution is:

$$\lambda_{\rm eff} = \frac{\int \lambda\, F(\lambda)\, \mathcal{B}(T,\lambda)\, {\rm d}\lambda}{\int F(\lambda)\, \mathcal{B}(T,\lambda)\, {\rm d}\lambda} \tag{26}$$

where $\mathcal{B}(T,\lambda)$ is the Planck function. In this area it is reported a third order polynomial fit to the behaviour of $\lambda_{\rm eff}$ with blackbody temperature:

$$\lambda_{\rm eff}(T) = a + bT_{\rm eff} + cT_{\rm eff}^2 + dT_{\rm eff}^3.$$

To limit the number of significant digits of the polynomial coefficients to three (for a compact writing of the expressions), the temperature must be parametrized. For ultraviolet and optical systems, the temperature is expressed as:

$$\theta = \frac{2500}{T({\rm K})} \tag{27}$$

and the polynomial fit

$$\lambda_{\rm eff}(T) = a_\theta + b_\theta\theta + c_\theta\theta^2 + {\rm d}_\theta\theta^3 \tag{28}$$

is computed over the interval 50 000 $\le T \le$ 2500 K. Within this range of temperatures the polynomial fits provide $\lambda_{\rm eff}(T)$ accurate to better than 3 Å for essentially all systems. For near-IR systems, the temperature is expressed as :

$$\Phi = \frac{500}{T({\rm K})} \tag{29}$$

and the polynomial fit

$$\lambda_{\rm eff}(T) = a_\Phi + b_\Phi\Phi + c_\Phi\Phi^2 + d_\Phi\Phi^3 \tag{30}$$

extends over the range 10 000 $\le T \le$ 500 K. Within it, the fit provides $\lambda_{\rm eff}(T)$ accurate to better than 0.01 μm for most systems. Finally, for far-IR systems, the temperature is expressed as:

$$\Psi = \frac{100}{T({\rm K})} \tag{31}$$

and the polynomial fit

$$\lambda_{\rm eff}(T) = a_\Psi + b_\Psi\Psi + c_\Psi\Psi^2 + d_\Psi\Psi^3 \tag{32}$$

is computed over the interval 3000 $\le T \le$ 100 K, where it provides results accurate to 0.02 μm for nearly all systems.

The coefficients in the polynomial fits are given explicitely even when null: for example, writing 0.00 for c_Ψ means that the actual coefficient of Ψ^2 is $|c_\Psi| < 0.005$ (0.005 being rounded to 0.01). The same applies to all other coefficients used in this paper (Sects. 3.1.4, 3.2.4 and 3.2.5).

3.1.4. Area ❹

The effective width $W_{\rm eff}$, in the case of a blackbody energy distribution, is the width of a rectangular bandpass of height 1.0, centered at $\lambda_{\rm eff}$, that collects from a blackbody $\mathcal{B}(T,\lambda)$ the same amount of energy going through the filter $f(\lambda)$:

$$\int f(\lambda)\, \mathcal{B}(T,\lambda)\, {\rm d}\lambda = \int_{\lambda_{\rm eff}-W_{\rm eff}/2}^{\lambda_{\rm eff}+W_{\rm eff}/2} \mathcal{B}(T,\lambda)\, {\rm d}\lambda. \tag{33}$$

Here it is provided a third order polynomial fit to the behaviour of $W_{\rm eff}$ with the blackbody temperature. The same parametrization of temperature (θ, Φ and Ψ) and ranges of applicability adopted for $\lambda_{\rm eff}(T)$ are mantained for $W_{\rm eff}(T)$ too.

The third order polynomial fits to $W_{\rm eff}(T)$ tipically provide results accurate to 5 Å for UV and optical systems, 0.01 μm for near-IR systems and 0.02 μm for far-IR ones.

3.2. Data scheme for reddening parameters

The behaviour with different reddening laws and amount of extinction is investigated in the remaining areas numbered in Fig. 4 for all photometric bands at $\lambda \le 8$ μm. The amount of extinction in a given band is :

$$A(\lambda) = -2.5 \lg \frac{\int F(\lambda)\, S(\lambda)\, \tau^\eta(\lambda)\, {\rm d}\lambda}{\int F(\lambda)\, S(\lambda)\, {\rm d}\lambda} \tag{34}$$

where $\tau(\lambda)$ is the transmission coefficient of the interstellar medium and η in the relative mass of the medium. The latter is taken so that a unit amount of medium ($\eta = 1$) causes a reddening $E_{B-V} = 1.0$ for O-type stars (Straižys 1992, p. 10, 100 and 136). In such a case the corresponding hydrogen column density is $N_{\rm H}({\rm HI} + {\rm H_2}) = 5.8 \times 10^{21}$ atoms cm^{-2} (Savage & Mathis 1979) for the average interstellar medium characterized by the standard $R_V = 3.1$ law.

Three extinction laws are considered, labelled according to their $R_V = A(V)/E_{B-V}$ ratio, as representative of the *continuum* of extinction laws encountered in Nature (from Fitzpatrick 1999). Their shapes are compared in Fig. 7. Their tabular version can be downloaded via

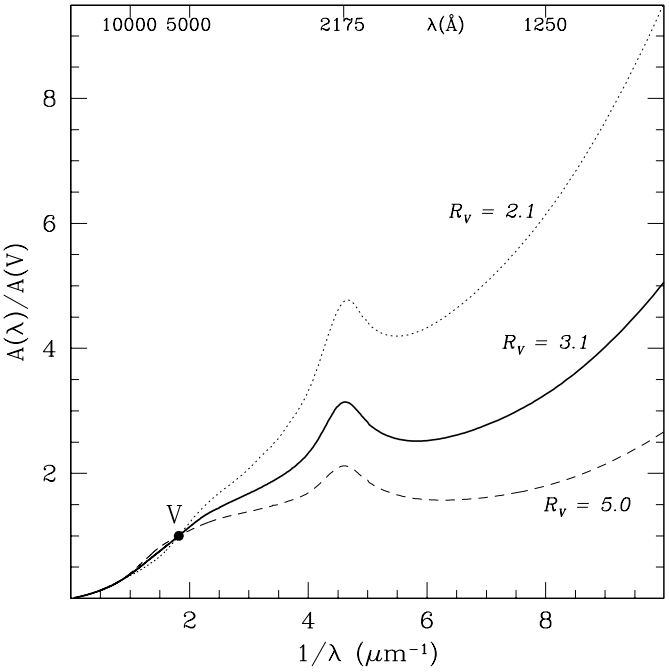

Fig. 7. The three extinction laws considered (from Fitzpatrick 1999). The dot marks the *V* band from the *UBV – Johnson and Morgan – 1953* system.

anonymous ftp from `astro2.astro.vill.edu` (directory *pub/fitz/Extinction/FMRCURVE.pro*) or from the ADPS *web* site.

The quantities normally employed in characterizing the effects of reddening and extinction in a given photometric system are color excess ratios $E(\lambda_4 - \lambda_3)/E(\lambda_2^{\rm ref} - \lambda_1^{\rm ref})$, ratios of total to selective extinction $A(\lambda)/E(\lambda_2^{\rm ref} - \lambda_1^{\rm ref})$, and absolute extinction ratios $A(\lambda)/A(\lambda^{\rm ref})$. Historically, the adopted $\lambda_i^{\rm ref}$ are the *B* and *V* bands of the *UBV – Johnson and Morgan – 1953* system. Such a choice may not be the optimal one because these bands are rather wide, they embrace a lot of fine structure features of the interstellar extinction and they are not on the R_V-independent part of the extinction curve at $\lambda \geq 8500$ Å. However, we will adopt *B* and *V* as $\lambda_i^{\rm ref}$ in this paper both for historical reasons and commonality with existing literature. In all computations we explicitely integrate over the whole and exact *B* and *V* profiles, and we do not limit ourselves to simply compute at the characteristic wavelength of the band.

Before to proceede, the *B* and *V* reference bands must be accurately defined. Throughout this paper we adopt for *B* and *V* the so called Vilnius reconstruction (Azusienis & Straižys 1969) of the original *UBV – Johnson and Morgan – 1953* system (hereafter Vilnius-rec-*UBV*; see Azusienis & Straižys 1969 for details on which *B* band to use in combination with *U* and *V* bands). The effect of choosing one or another band profile for the reference *B* and *V* bands has non-negligible effects. Table 2 (built from data in Figs. 12, 61 and 131, for the $R_V = 3.1$ extinction law and the B3 spectral type) shows the differences between the USA, Vilnius, photographic, Buser (1978), Bessell (1990) and Landolt (1983) versions of the same *UBV – Johnson and Morgan – 1953* system. It is evident how

Table 2. Values of the reddening parameters $A(\lambda)/A(V)$ and $A(\lambda)/E_{B-V}$ for different reconstructions of the *V* band of the *UBV – Johnson and Morgan – 1953* photometric system. The reference *B* and *V* bands are those of the Vilnius reconstruction. The reconstruction by Buser (1978) adopts the same reconstruction as Vilnius for the *V* band, which explains the identical numbers for the two.

reconstruction	$\frac{A(V)}{A(V)}$	$\frac{A(V)}{E_{B-V}}$
Vilnius	1.00	$3.132 + 0.022\times E_{B-V}$
USA	0.98	$3.104 + 0.021\times E_{B-V}$
photographic (103a-G)	1.03	$3.165 + 0.039\times E_{B-V}$
photographic (103a-D)	0.92	$3.000 + 0.005\times E_{B-V}$
Bessell	0.99	$3.126 + 0.022\times E_{B-V}$
Buser	1.00	$3.132 + 0.022\times E_{B-V}$
Landolt	1.01	$3.164 + 0.022\times E_{B-V}$

the differences cannot be ignored when an accurate analysis is required.

It has to be noted that the reddening expressions depend on the spectral type of the star and the amount of reddening because both change the band effective wavelengths. An example illustrates the effect of the stellar spectral type. For Vilnius-rec-*UBV* in Fig. 12b, $R_V = 3.1$ law and $\eta = 1$ in Eq. (34), the effective wavelengths of the $A(V)/E_{B-V}$ ratio for a B3 star are:

$$\frac{A(V)}{E_{B-V}} \longrightarrow \frac{A(5429\ \text{Å})}{E(4336-5429\ \text{Å})}$$

while for a M2 star they become:

$$\frac{A(V)}{E_{B-V}} \longrightarrow \frac{A(5595\ \text{Å})}{E(4666-5595\ \text{Å})}.$$

Going from spectral type B3 to M2, the $\lambda_{\rm eff}$ of the *B* band changes by 330 Å while for the *V* band the change is only 166 Å. The lever arm (i.e. the distance in $\lambda_{\rm eff}$ between *B* and *V* bands) reduces toward redder spectral types, therefore requiring a higher $A(V)$ extinction to match the $E_{B-V} = 1.0$ condition. From data in Fig. 12b it is in fact:

$$\begin{aligned}\frac{A(V)}{E_{B-V}} &= 3.13 \text{ for early type stars}\\ &= 3.31 \text{ for Sun – like stars}\\ &= 3.69 \text{ for M stars.}\end{aligned}$$

The effect of the reddening is also quite strong. Again from Fig. 12b for Vilnius-rec-*UBV*, a $\triangle E_{B-V} = 1.0$ changes the effective wavelength of the *B* band by 133 Å, and that of the *V* band by 113 Å.

The net effect is that the reddening does not translate rigidly the main-sequence over the color-magnitude diagram: the shape of the main-sequence modifies according to the amount of reddening (with obvious implications for classical reddening estimates of clusters). How much the main-sequence shape modifies for different amounts of reddening is grafically represented in Fig. 8 for the *UBVRI – Landolt – 1983* system

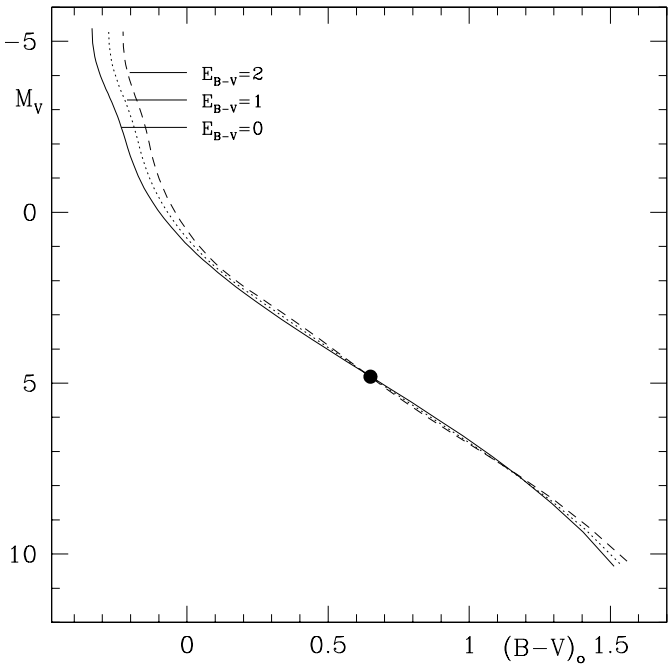

Fig. 8. Modification of the main-sequence on the M_V, $(B-V)_\circ$ plane of the *UBVRI – Landolt – 1983* system for the $R_V = 3.1$ extinction law and different reddenings (E_{B-V} = 0,1,2) . The curves are shifted so that the solar positions for them coincide (dot). Nearly identical modifications apply for the $R_V = 5.0$ and $R_V = 2.1$ cases. The unreddened main-sequence is from Drilling & Landolt (2000, their Table 15.7).

(the curves are available in electronic form from the ADPS web site).

3.2.1. Area ❺

The $A(\lambda)/A(V)$ absolute extinction ratio

$$\left.\frac{A(\lambda)}{A(V)}\right|_{R_V} = X.XX\ \frac{Q_1}{Q_2} \tag{35}$$

is reported in this area for the pure band transmission profile, without covolution with a source spectrum and for $\eta = 1$ (cf. Eq. (34)). The ratio is computed for the three different extinction laws labelled by their R_V values.

The covolution with a source spectrum modifies however the value of the ratio: the extremes reached over the sources considered in *area* ❷ are listed as values Q_1 and Q_2 in the equation scheme above. For optical systems only spectra of normal stars (cf. Sect. 2) are considered.

3.2.2. Area ❻

The shape of the extinction law $A(\lambda)/A(V)$ can be conveniently and accurately parametrized in term of R_V as :

$$\frac{A(\lambda)}{A(V)} = a(x) + \frac{b(x)}{R_V} \tag{36}$$

where $x = 1/\lambda$ (in μm^{-1}). The analytical expressions of $a(x)$ and $b(x)$ coefficients are given by Cardelli et al. (1989). They offer a powerful way to derive the extinction at any wavelength for any extinction law parametrized by R_V.

The $a(x)$ and $b(x)$ coefficients can be profitably used to parametrize in terms of R_V the reddening relations normally used :

$$\frac{E(\lambda_2-\lambda_1)}{A(V)} = (a_2-a_1) + \frac{(b_2-b_1)}{R_V} \tag{37}$$

$$\frac{A(\lambda)}{E_{B-V}} = \frac{A(\lambda)}{A(V)}R_V = aR_V + b \tag{38}$$

$$\frac{E(\lambda-V)}{E_{B-V}} = \frac{A(\lambda)}{E_{B-V}} - R_V = (a-1)R_V + b \tag{39}$$

$$\frac{E(\lambda_2-\lambda_1)}{E_{B-V}} = (a_2-a_1)R_V + (b_2-b_1). \tag{40}$$

These relations show that expressing the extinction in terms of $A(\lambda)/A(V)$ or $E(\lambda-V)/E_{B-V}$ is equivalent, provided that R_V is known. If the extinction law is unknown, $A(\lambda)/A(V)$ and $E(\lambda-V)/E_{B-V}$ cease to be equivalent ways to describe the extinction.

The values of $a(x)$ and $b(x)$ depend on the source spectrum and the amount of reddening because both change the $\lambda_{\rm eff}$ at which the coefficients are computed. For example, for the *R* band of the *UBVRI – Landolt – 1983* system, it is $\triangle\lambda_{\rm eff}$ = 124 Å when moving from B3 to Sun spectral type, and $\triangle\lambda_{\rm eff}$ = 264 Å when changing from $E_{B-V} = 0.0$ to $E_{B-V} = 1.0$. Such variations are too large to be ignored, and therefore we have computed the $a(x)$ and $b(x)$ coefficients for the *B*3 and *Sun* spectral types (representative of the hotter and cooler regions of the HR diagram, respectively) for both $E_{B-V} = 0.0$ and $E_{B-V} = 1.0$ conditions. They are given in area ❻ in the following format:

for $E_{B-V} = 0.0 \rightarrow$	$a = ^{x.xxx}_{x.xxx}$	$b = ^{x.xxx}_{x.xxx}$	*B3*
for $E_{B-V} = 1.0 \rightarrow$			
for $E_{B-V} = 0.0 \rightarrow$	$a = ^{x.xxx}_{x.xxx}$	$b = ^{x.xxx}_{x.xxx}$	*Sun*
for $E_{B-V} = 1.0 \rightarrow$			

The $a(x)$ and $b(x)$ coefficients are useful also in deriving *Q* or *reddening-free* parameters for any extinction law characterized by R_V. A reddening-free parameter is a combination of colors that is independent from interstellar reddening. Given four photometric bands *A*, *B*, *C* and *D*, the reddening-free parameter and its expression in terms of $a(x)$ and $b(x)$ coefficients are:

$$\begin{aligned} Q_{ABCD} &= (A-B) - \frac{E_{A-B}}{E_{C-D}}(C-D) \\ &= (A-B) - \frac{(a_A-a_B)R_V + (b_A-b_B)}{(a_C-a_D)R_V + (b_C-b_D)}(C-D). \end{aligned} \tag{41}$$

Because $a(x)$ and $b(x)$ depend upon the effective wavelength, the Q_{ABCD} so derived will be most accurate only in the neighborhood of a given spectral type and for a given amount of reddening.

The best known reddening-free parameter is perhaps that for the *UBV – Johnson and Morgan – 1953* system, given by Hiltner & Johnson (1956) as $Q_{UBV} = (U-B) - \Upsilon(B-V)$ where $\Upsilon = 0.72 + 0.05E_{B-V}$ for O-type stars suffering from a standard $R_V = 3.1$ extinction law. Using the values of $a(x)$ and $b(x)$ from Fig. 12b (Vilnius-rec-*UBV*) for the B3 spectral type,

Eq. (49) provides $\Upsilon = 0.71$ for $E_{B-V} = 0.0$ and $\Upsilon = 0.78$ for $E_{B-V} = 1.0$, in excellent agreement with Hiltner and Johson's values. The corresponding figures for a *Sun*–like source spectrum would be instead $\Upsilon = 0.88$ for $E_{B-V} = 0.0$ and $\Upsilon = 1.06$ for $E_{B-V} = 1.0$.

3.2.3. Area ❼

In this area it is given the second order polynomial fit to extinction versus reddening for the $R_V = 3.1$ extinction law and three different spectral types according to the wavelength region: B3, Sun and M2 for optical and infrared systems, and ι Her (B3), Sun and a Kurucz's 40 000 K, $[Z/Z_\odot] = 0.0$, $\lg g = 5.0$ spectrum for ultraviolet systems. The coefficients are given in the form:

$$\frac{A(\lambda)}{E_{B-V}} = \alpha + \beta E_{B-V} = (\alpha, \beta)^r_{\rm spectrum}. \quad (42)$$

The expression provides an exact solution, in the sense that the absorption in the three bands B, V and λ is computed for each incremental value of x in Eq. (34). The regression coefficient r gives as an indication of the accuracy of the fit (generally pretty high with $|r|$ close to 1.0).

The α and β coefficients can be used to derive the reddening-free parameter Q_{ABCD} in a direct way (for the $R_V = 3.1$ law, while for others it is necessary to use Eq. (49) above):

$$Q_{ABCD} = (A - B) - \frac{E_{A-B}}{E_{C-D}}(C - D) \quad (43)$$
$$= (A - B) - \frac{\alpha_A - \alpha_B + (\beta_A - \beta_B)E_{B-V}}{\alpha_C - \alpha_D + (\beta_C - \beta_D)E_{B-V}}(C - D).$$

From the α and β coefficients in Fig. 12b in the VILNIUS-REC-*UBV* case and B3 spectral type, it is found $\Upsilon = 0.70 + 0.05E_{B-V}$ for $Q_{UBV} = (U - B) - \Upsilon(B - V)$, again in excellent agreement with Hiltner & Johnson (1956) value for O-type stars.

3.2.4. Area ❽

In this area it is reported the first order polynomial fit to the behaviour of $\lambda_{\rm eff}$ with E_{B-V} for the pure band transmission profile and the $R_V = 3.1$ extinction law:

$$\lambda_{\rm eff} = \delta + \gamma E_{B-V}. \quad (44)$$

The regression coefficient r is given as an indication of the accuracy of the fit.

3.2.5. Area ❾

Similarly, a first order polynomial fit to the behaviour of $W_{\rm eff}$ with E_{B-V} for the pure band transmission profile and the $R_V = 3.1$ extinction law is given:

$$W_{\rm eff} = \varepsilon + \zeta E_{B-V}. \quad (45)$$

Again, the regression coefficient r is given as an indication of the accuracy of the fit.

4. Additional photometric systems

The 17 new photometric systems added to the ADPS are here briefly noted. The wavelength and width of the bands listed in this section (including terminology and number of decimal figures) are those given in the original papers, while wavelengths and widths given in the rest of this paper (electronic Figs. 9–187) come from our computations based on the actual band profiles. The new systems with available band transmission profiles are:

Strömgren and Gyldenkerne – 1955 (Fig. 15). From a series of 25 interference filters with transmission peaks in the range 3800–5500 Å used to measure 110 MKK standard stars at the Observatoire de Haute-Provence, a first group of four filters was isolated and used by Strömgren (1956) to define his *uvby* system aiming to study F stars (and later extended to A and B types). A second group of five filters was selected by Strömgren & Gyldenkerne (1955) to become the base of a system designed to measure G and K stars, in particular the CaII-K line, the discontinuity at the *G*-band and CN intensity. The adopted bands have widths at half maximum of 100 Å and central wavelengths at 3910, 4030, 4170, 4240 and 4360 Å.

Bahner – 1963 (Fig. 31). A system composed by 16 square bands in the range 3200–6400 Å aimed to investigate B and A stars. Four bands are devoted to the measurement of the Balmer continuum, and ten bands to the optical continuum away from strong absorption features.

Mould and Wallis – 1977 (Fig. 103). In ADPS I we briefly mentioned it as a modification of the *Mould – 1976* system. Actually, the differences are large enough to justify its inclusion in ADPS II as a separate photometric system. It is aimed to the measurement of CaH and TiO bands in M stars and T Tau stars of the M spectral type. Five bands, realized with interference filters, have their central wavelengths (and widths at half maximum) at 5450 (200), 6940 (140), 7140 (140), 7520 (140) and 8500 (400) Å.

Malyuto et al. – 1997 (Fig. 142). This is a system with six sets of bands, each one composed by three square bands, aimed to quantitatively classify K and M stars via the strengh of FeI (+TiO α_1) around 5013, Mg*b* (+TiO α_0) at 5235, NaI D (+TiO γ'_1) at 5930, TiO γ_0 at 7235, TiO γ'_0 6250 and TiO γ_1 6723 Å bands. The bands are realized on spectra and are found to be insensitive to differences in data reduction procedures, reddening and resolution of the spectral catalogues to which they are applied. The system is claimed to provide an average accuracy of 0.6 spectral subtype and 0.8 luminosity class in the classification of K and M stars.

Hickson and Mulrooney – 1998 (Fig. 145). A survey of 20 deg^2 in 33 narrow bands complete to mag ∼20 has been conducted with the 3-m liquid mirror telescope of the NASA Orbital Debris Observatory. The filters have central wavelengths ranging from 4545 to 9477 Å, at intervals of ∼0.01 in $\lg\lambda$, and give a resolving power of $\lambda/\Delta\lambda \sim 44$. The survey aims to provide photometric redshifts of ∼10^4 galaxies and QSOs and accurate photometry and spectral classification for ∼10^4 field stars. Central wavelengths (and bandwidths) of the photometric bands (in Å) are: 4545 (177), 4659 (185), 4756 (193), 4860 (202), 4981 (219), 5102 (224), 5190 (227), 5327

(228), 5451 (210), 5570 (214), 5711 (217), 5856 (231), 5976 (243), 6137 (236), 6287 (264), 6411 (240), 6546 (280), 6713 (291), 6880 (292), 7044 (299), 7187 (306), 7347 (322), 7524 (332), 7696 (319), 7875 (333), 8059 (346), 8248 (337), 8438 (356), 8679 (351), 8831 (413), 9063 (353), 9245 (400) and 9477 (391).

JHK KPNO – Manduca and Bell – 1979 (Fig. 162). The transmission of the *JHK* filters in use at KPNO are given together with local Earth's atmosphere transmission.

KAO far-IR – Harvey – 1979 (Fig. 163). This is the five bands, far-IR photometric system for the He-cooled bolometer attached to the 0.91 m telescope on board the Kuiper Airborne Observatory airplane. The bolometer explores the range of wavelengths blocked by the Earth's atmosphere longward of 35 μm. The $\lambda_{\rm eff}$ and widths at half maximum (for a Sun-like energy distribution as reflected by a planetary surface) of the five bands are (in μm): 40 and 31–49 (band *KAO-40*); 52 and 44–59 (*KAO-52*); 100 and 80–130 (*KAO-100N*); 110 and 80–155 (*KAO-100B*); 160 and 125–250 (*KAO-160*).

IRTS FIRP – Lange et al. – 1994 (Fig. 173). The Far-IR Photometer (FIRP) on the IR Telescope in Space (IRTS) provided absolute photometry in four bands, whose central wavelengths (and widths at half maximum) are: 150 (68), 250 (135), 400 (130) and 700 (370) μm.

S-520-15 FIR – Matsuhara et al. – 1994 (Fig. 174). A five bands, far-IR photometer was placed aboard a S-520-15 rocket launched on Feb. 2, 1992 by ISAS (Japan) from the Kagoshima Space Center. The He-cooled telescope aimed to the detection of diffuse far-IR emission at high galactic latitudes during the 350 s flight outside the atmosphere. It carried both wide bands (*BC1*, *BC2* and *BC3*) and narrow ones, the latter's goal being the detection of diffuse emission in the [CII] line at 157.7 μm (a narrow *LC* band at the line nominal wavelength, and an associated control *CC* band on the adjacent continuum). The central wavelengths and widths at half maximum of the bands are (in μm): 95 and 19 (band *BC1*); 134 and 13 (*BC2*); 186 and 23 (*BC3*); 157.9 and 1.3 (*LC*); 153.7 and 1.5 (*CC*).

iz, iJ, iH, iK, iL, iL′, iM, in, iN, iQ – Young et al. – 1994 (Fig. 177). It is the optimization of infrared bands by Young et al. (1994) in response to recommendations made by the Working Group on Infrared Extinction and Standardization of IAU Commission 25. The optimization aims to enhance reproducibility and trasformability and to allow the use of linear extinction curves by reducing the effect of molecular absorption at the edges of the photometric bands. Peak weavelengths and widths at half maximum are (in μm): 1.032 and 0.073 (band *iz*); 1.240 and 0.079 (*iJ*); 1.628 and 0.152 (*iH*); 2.196 and 0.188 (*iK*); 3.620 and 0.274 (*iL*); 3.900 and 0.274 (*iL′*); 4.675 and 0.114 (*iM*); 9.030 and 0.323 (*in*); 11.10 and 2.00 (*iN*); 17.90 and 1.61 (*iQ*).

ABU SPIREX – 1998 (Fig. 181). A six band photometric system is available at the 60-cm telescope of the SPIREX facility at the South Pole, operated by the Center for Astrophysical Research in Antartica (CARA) and NOAO (Fowler et al. 1998 and `http://www.noao.edu/scopes/south_pole/`). The bands have their central wavelength and width at half-maximum as follow (in μm): 2.4245 and 2.4076–2.4414 (band *$H_2Q(3)$*); 3.299 and 3.262–3.336 (*PAH*); 3.514 and 3.205–3.823 (*L*); 3.821 and 3.520–4.122 (*L′*); 4.051 and 4.024–4.078 (*Br*α); 4.668 and 4.586–4.749 (M_N).

JHK′K_sKL′M′ MKO – Tokunaga et al. – 2002 (Fig. 182). The new set of near-IR filters for the Mauna Kea Observatories (MKO) is designed to avoid as much as possible the detrimental effects of telluric absorption bands, to the aim of reducing background noise, improving photometric transformations between Observatories, providing greater accuracy in extrapolating to zero airmass, and reducing the color dependence of extinction coefficients. The central wavelengths and widths at half maximum (in μm) for the seven bands are (Tokunaga et al. 2002): 1.250 and 1.170–1.330 (band *J*); 1.635 and 1.490–1.780 (*H*); 2.120 and 1.950–2.290 (*K′*); 2.150 and 1.990–2.310 (K_s); 2.200 and 2.030–2.370 (*K*); 3.770 and 3.420–4.120 (*L′*); 4.680 and 4.570–4.790 (*M′*).

The new systems censed in the ADPS that have no documentation about their band transmission profiles (and that are therefore not further considered in this paper) are:

Aerobee IR-65 – 1965. An Aerobee rocket carrying a N_2−cooled telescope was launched on Oct 29, 1965 for a scan of the sky during a ∼300 s ballistic flight outside the atmosphere. Two photometric bands were realized: *InAs* with a band-pass from 1 to 3 μm and *AuGe* with a band-pass from 3 to 7 μm (McNutt et al. 1966; Harwit et al. 1966).

DIRBE COBE – Kelsall et al. – 1990. DIRBE is an absolute photometer on COBE (COsmic Background Explorer). It is internally stabilized to 1% repeatibility and it is equipped with 10 infrared bands. They are the *J*(1.25 μm), *K*(2.3), *L*(3.5) and *M*(4.5) bands, plus the IRAS bands nominally at 12, 25, 60 and 100 μm, and two additional bands at 160 and 240 μm.

SpaceLab IRT – Kent et al. – 1992. Survey scans of the sky at six infrared wavelengths were obtained with IRT (infrared telescope experiment), as part of the SpaceLab-2 mission on the Space Shuttle 51-F. The six bands have width at half maximum (in μm) of 1.7–3.0, 4.5–9.5, 6.1–7.1, 8.5–14, 18–30 and 70–120. Data collected at $\lambda > 3$ μm were corrupted by the high background radiation generated by the Shuttle environment. Data from the shortest band were instead useful in producing a map of the Galaxy emission at 2.4 μm. The single-band photometric system is defined by the flux of three reference stars (g Her, α Her and μ Cep).

MSX – Egan and Price – 1996. The infrared telescope radiometer (SPIRIT III) aboard the Ballistic Missile Defense Organization (BMDO) Mid-course Space Experiment (MSX) has been used to pinpoint infrared astrometric reference stars (177 860 sources cataloged, Egan & Price 1996). The radiometer includes six photometric bands whose mean wavelengths and widths at half maximum are (in μm): 4.29 and 4.22–4.36 (band B_1); 4.35 and 4.24–4.46 (B_2); 8.26 and 6.0–10.9 (*A*); 12.1 and 11.1–13.2 (*C*); 14.7 and 13.5–16.0 (*D*); 21.4 and 18.1–26.0 (*E*).

TIRCAM 2 – Persi et al. – 2002. Mid-IR photometric system for the TIRGO Infrared Observatory, defined by the flux at 1.0 airmass of six reference stars (α Lyr, β Gem, α Boo, β And, β Peg and α Tau) as given in Persi et al. (2002). $\lambda_{\rm eff}$ and widths at half maximum are (in μm): 8.81 and 8.4–9.2 (band *F[8.8]*); 9.80 and 9.3–10.3 (*F[9.8]*); 10.27 and 9.8–10.8

(*F[10.3]*); 11.69 and 11.1–12.3 (*F[11.7]*); 12.49 and 11.9–13.1 (*[F12.5]*). The TIRCAM 2 is an upgrade of a previous TIRCAM 1 (Persi et al. 1996) version.

5. Notes on individual photometric systems

UBV – Johnson and Morgan – 1953 (Fig. 12). Compared to Paper I, a fourth system reconstruction has been considered (Buser 1978; Buser & Kurucz 1978), while Vilnius one for the B band is now properly splitted into the B and B_p variants (cf. Strayžis 1992).

PV – Eggen – 1955 (Fig. 14). The wavelength and width of the V filter as given in Paper I are inaccurate.

Vilnius – Straižys et al. – 1965 (Fig. 38). The transmission curves for S and T filters are taken from Straižys (1992).

27 colors – Wing – 1967 (Fig. 49). In accordance to Paper I, we consider here only the bands for which λ_c is specified in the source paper.

Hβ, γ – Sinnerstad et al. – 1968 (Fig. 52) The overall shape of the Hβ-wide filters is taken equivalent to Hγ-wide as specified in the source paper.

Spinrad and Taylor – 1969 (Fig. 56). The widths of the bands (16 Å shortward of 5360 Å and 32 longward) as revised by Spinrad & Taylor (1971) are adopted here.

nh – Landolt – 1970 (Fig. 61). Only the Oct 14, 1965 filter set is considered.

Hγ – Häggkvist – 1971 (Fig. 64). The source paper reports about aging effects on wavelengths and widths of the adopted interference filters. Mean values are considered here.

Wawrukiewicz – 1971 (Fig. 68). Actual $FWHM$ of TiO bands are twice the values reported in Paper I.

Caplan – 1973 (Fig. 76). Bands *6548* and *6577* given in Paper I are actually a single band extending from 6536 to 6589 Å.

10 colors – Faber – 1973 (Fig. 79). Band transmission profiles are taken from Fig. 1 of the source paper.

Hα – Vidal – 1974 (Fig. 89). Paper I reports right values for band $FWHM$, but plots and tabulates them twice as large.

uvgr 39_B 39_N – Zinn – 1980 (Fig. 109). The *uvgr* bands are the same as those of the *uvgr – Thuan and Gunn – 1976* system (see Fig. 100), and therefore only the 39_B and 39_N interference filter bands are considered here.

eight-colors – Tedesco et al. – 1982 (Fig. 116). Band transmission profiles are taken from Fig. 1 of the source paper.

Kenyon and Fernandez-Castro – 1987 (Fig. 125). Differently from Paper I, here we consider also the two bands at 8190 and 8400 Å described in the source paper.

$g_4r_4i_4z_4$ – Schneider et al. – 1989 (Fig. 129). Paper I reports erroneous transmission curves, that have been replaced by the correct ones in the ADPS web site and in this paper.

Hipparcos – 1989 (Fig. 130). Besides the original ESA's transmission curves (as published in the Hipparcos Catalogue, ESA SP-1200), here we consider also the revised profiles by Bessell (2000).

POSS II – Reid et al. – 1991 (Fig. 133). Paper I reports erroneous transmission curves, that have been replaced by the correct ones in the ADPS web site and in this paper.

TNG – Marchetti et al. – 1997 (Fig. 143). Band transmission curves are derived from Fig. 1 of the source paper.

UWTAT – Strassmeier et al. – 1997 (Fig. 144). The photometric system combines bands from other systems (*uvby* Hβ *– Strömgren and Crawford – 1956*, *UBV – Johnson and Morgan – 1953*, R_cI_c *– Cousins – 1976*, Hα,β *– Guinan and McCook – 1974*). Here we adopt the band transmission curves derived from Fig. 4 of the source paper.

Geneva GAIA – Grenon et al. – 1999 (Fig. 148). The provisional band profiles adopted in Paper I are here replaced by the proper ones (C. Jordi, private communication).

OAO2 WEP – 1970 (Fig. 151). Filter names have been revised according to post-lunch documentation (Wende 1974). Filters *213, 256, 297, 333* are here ignored because associated to the nebular photometer that failed shortly after launch.

UIT – 1990 (Fig. 156). Paper I reports erroneous transmission curves, that have been replaced by the correct ones in the ADPS web site and in this paper.

Pilachowski – 1978 (Fig. 161). We have neglected the wide band at 2.2 μm because it is a standard K band.

Acknowledgements. M.F. has been financially supported by ASI via contract CISAS 10/2001 to P. L. Bernacca. Dina Moro is kindly acknowledged for her careful documentation of all references used in Paper I, without which the preparation of this Paper II would have been even more laborious. The anonymous referee is thanked for constructive and detailed comments and close scrutiny of the paper.

References

Argue, A. N. 1967, MNRAS 135, 23
Azusienis, A., & Straižys V. 1969, Soviet Astron., 13, 316
Bahner, K. 1963, ApJ, 138, 1314
Bessell, M. S. 1990, PASP, 102, 1181
Bessell, M. S. 2000, PASP, 112, 961
Borgman, J. 1960, BAN, 15, 255
Buser, R. 1978, A&A, 62, 411
Buser, R., & Kurucz R. L. 1978, A&A, 70, 555
Canterna, R. 1976, AJ, 81, 228
Caplan, J. G., 1973, A&A, 28, 213
Cardelli, J. A., Clayton, G. C., & Mathis, J. S. 1989, ApJ, 345, 245
Castelli, F., Parthasarathy, M., & Hack, M. 1997, A&A, 321, 254
Crawford, D. L. 1958, ApJ, 128, 185
Crawford, D. L. 1960, ApJ, 132, 66
Crawford, D. L., & Mander J. 1966, AJ 71, 114
Crawford, D. L., & Barnes J. V. 1970, AJ 75, 978
Drilling, J. S., & Landolt, A. U. 2000, in Allen's Astrophysical Quantities, ed. A.N. Cox (AIP Press, Springer) 381
Egan, M. P., & Price, S. D. 1996, AJ, 112, 2862
Eggen, O. J. 1955, AJ, 60, 65
Epchtein, N., de Batz B., Copet E., et al. 1994, Ap&SS, 217, 3
Faber, S. M. 1973, A&AS, 10, 201
Fitzpatrick, E. L. 1999, PASP 111, 63
Fowler, A.M., Sharp N., Ball W., et al. 1998, SPIE, 3354, 1170
Fukugita, M., Ichikawa T., Gunn J. E., et al. 1996, AJ, 111, 1748
Golay, M. 1974, Introduction to astronomical photometry, Ap&SS Lib. 41 (Dordrecht: Reidel Publishing Company, Holland)
Grenon, M., Jordi, C., Figueras F., & Torra J. 1999, technical report to the ESA's GAIA Photometric Working Group (MG-PWG-002)
Häggkvist, L. 1971, A&A, 12, 5
Harvey, P. M. 1979, PASP, 91, 143

Harwit, M., McNutt, D. P., Shivanandan, K., et al. 1966, AJ, 71, 1026
Hickson, P., & Mulrooney, M. K. 1998, ApJS, 115, 35
Hiltner, W. A., & Johnson, H. J. 1956, ApJ, 124, 367
Johnson, H. L., & Morgan, W. W. 1953, ApJ, 117, 313
Kelsall, T., Hauser, M. G., Pedelty, J. A., et al. 1990, BAAS, 22, 886
Kent, S. M., Mink, D., Fazio, G., et al. 1992, ApJS, 78, 403
Kenyon, S. J., & Fernandez-Castro, T. 1987, AJ, 93, 938
Landolt, A. U. 1970, AJ, 75, 337
Landolt, A. U. 1983, AJ, 88, 439
Lange, A. E., Freund, M. M., Sato, S., et al. 1994, ApJ, 428, 384
Low, F. J., & Rieke, G. H. 1974, in Methods of Experimental Physics, 12, Part A, ed. N. Carleton (New York: Academic Press) 456
Malyuto, V., Oestreicher, M. O., & Schmidt-Kaler, Th. 1997, MNRAS, 286, 500
Manduca, A., & Bell, R. A. 1979, PASP, 91, 848
Marchetti, E., Mallucci, S., Ghedina, A., et al. 1997, in The Three Galileos: the Man, the Spacecraft, the Telescope, ed. C. Barbieri, J. H. Rahe, T. V. Johnson, & A. M. Sohus, (Kluwer Academic Publishers, Ap&SS Lib. 220, 383
Matsuhara, H., Kawada, M., Matsumoto, T., et al. 1994, PASJ, 46, 665
McClure, R. D., & Van den Bergh, S. 1968, AJ, 73, 313
McNutt, D. P., Shivanandan K., Zajac, B. J., et al. 1966, AJ, 71, 170
Moro, D., & Munari, U., 2000, A&AS 147, 361 (Paper I)
Mould, J. R. 1976, ApJ, 207, 535
Mould, J. R., & Wallis, R. E., 1977, MNRAS, 181, 625
Munari, U., & Zwitter, T. 2002, A&A, 383, 188
Persi, P., Busso, M., Corcione, L., et al. 1996, A&A, 306, 587
Persi, P., Busso, M., Corcione, L., et al. 2002, in Solids and Molecules in Space, ed. C. Cecchi-Pestellini & S. Aniello, Ital. Phys. Soc. Conf. Proc. series, in press
Pilachowski, C. A. 1978, ApJ, 224, 412
Press, V. H., Teukolsky, S. A., Vetterling, W. T., et al. 1988, Numerical Recipes in C (Cambridge: Cambridge University Press)
Reid, I. N., Brewer, C., Brucato, R. J., et al. 1991, PASP, 103, 661
Savage, B. D., & Mathis, J. S. 1979, ARA&A, 17, 73
Schneider, D. P., Schmidt, M., & Gunn, J. E. 1989, AJ, 98, 1507
Sinnerstad, U., Arkling, J., Alm, S. H., et al. 1968, Ark. Astr., 5, 105
Spinrad, H., & Taylor, B. J. 1971, ApJS, 22, 445
Straižys V., & Zdanavičius K. 1965, Bull. Vilnius Obs. 14,1
Straižys V. 1973, A&A, 28, 349
Straižys V. 1992, Multicolor Stellar Photometry (Pachart Publishing House, Tucson, Arizona)
Strassmeier, K. G., Boyd, L. J., Epand, D. H., et al. 1997, PASP, 109, 697
Strömgren B. 1956, Vistas in Astron., 2, 1336
Strömgren B. 1963, in Basic Astronomical Data, ed. K. A. Strand (Univ. Chicago Press), 123
Strömgren B. 1966, ARA&A, 4, 433
Strömgren B., & Gyldenkerne K. 1955, ApJ, 121, 43
Tedesco, F. E., Tholen, D. J., & Zellner, B. 1982, AJ, 87, 1585
Tokunaga, A. T., Simons, D. A., & Vacca, W. D. 2002, PASP, 114, 180
Vidal, J.-L. 1974, A&A, 34, 401
Wawrukiewicz, A. S. 1971, PASP, 83, 57
Wende, C. D. 1974, OAO 2/Wisconsin Experiment Package (WEP) Photometric Users Guide, NASA NSSDC, 74-02
Wing, R.F. 1967, in Colloq. on Late-Type Stars, ed. M. Hack, Trieste Astron. Obs., 205
Young, A. T., Milone, E. F., & Stagg, C. 1994, A&AS, 195, 259
Zinn, R. 1980, ApJS, 42, 19